

Full-field reconstruction of ultrashort waveforms by time to space conversion interferogram analysis

Dror Shayovitz,^{1,*} Harald Herrmann,² Wolfgang Sohler,² Raimund Ricken,² Christine Silberhorn,² and Dan M. Marom¹

¹Department of Applied Physics, Hebrew University of Jerusalem, Jerusalem, 91904, Israel

²Department of Applied Physics, The University of Paderborn, Warburger Str. 100 D-33098, Paderborn, Germany

*dror.shayovitz@mail.huji.ac.il

Abstract: Accurate amplitude and phase measurements of ultrashort optical waveforms are essential for their use in a wide range of scientific disciplines. Here we report the first demonstration of full-field optical reconstruction of ultrashort waveforms using a time-to-space converter, followed by a spatial recording of an interferogram. The algorithm-free technique is demonstrated by measuring ultrashort pulses that are widely frequency chirped from negative to positive, as well as phase modulated pulse packets. Amplitude and phase measurements were recorded for pulses ranging from 0.5 ps to 10 ps duration, with measured dimensionless chirp parameter values from -30 to 30 . The inherently single-shot nature of time-to-space conversion enables full-field measurement of complex and non-repetitive waveforms.

©2014 Optical Society of America

OCIS codes: (320.0320) Ultrafast optics; (190.0190) Nonlinear optics.

References and links

1. C. I. Blaga, J. Xu, A. D. DiChiara, E. Sistrunk, K. Zhang, P. Agostini, T. A. Miller, L. F. DiMauro, and C. D. Lin, "Imaging ultrafast molecular dynamics with laser-induced electron diffraction," *Nature* **483**(7388), 194–197 (2012).
2. B. E. Van Kuiken, N. Huse, H. Cho, M. L. Strader, M. S. Lynch, R. W. Schoenlein, and M. Khalil, "Probing the electronic structure of a photoexcited solar cell dye with transient x-ray absorption spectroscopy," *J. Phys. Chem. Lett.* **3**, 1695–1700 (2012).
3. R. S. Pillai, C. Boudoux, G. Labroille, N. Olivier, I. Veilleux, E. Farge, M. Joffre, and E. Beaufaire, "Multiplexed two-photon microscopy of dynamic biological samples with shaped broadband pulses," *Opt. Express* **17**(15), 12741–12752 (2009).
4. W. Ng, T. D. Rockwood, G. A. Sefler, and G. C. Valley, "Demonstration of a large stretch-ratio ($M = 41$) photonic analog-to-digital converter with 8 ENOB for an input signal bandwidth of 10 GHz," *IEEE J. Photon. Technol. Lett.* **24**(14), 1185–1187 (2012).
5. T. Richter, E. Palushani, C. Schmidt-Langhorst, R. Ludwig, L. Molle, M. Nölle, and C. Schubert, "Transmission of Single-Channel 16-QAM Data Signals at Terabaud Symbol Rates," *J. Lightwave Technol.* **30**(4), 504–511 (2012).
6. J. T. Willits, A. M. Weiner, and S. T. Cundiff, "Line-by-line pulse shaping with spectral resolution below 890 MHz," *Opt. Express* **20**(3), 3110–3117 (2012).
7. D. J. Kane and R. Trebino, "Single-shot measurement of the intensity and phase of an arbitrary ultrashort pulse by using frequency-resolved optical gating," *Opt. Lett.* **18**(10), 823–825 (1993).
8. D. J. Kane, R. Trebino, K. W. DeLong, D. N. Fittinghoff, J. N. Sweetsier, M. A. Krumbugel, and B. A. Richman, "Measuring ultrashort laser pulses in the time-frequency domain using frequency-resolved optical gating," *Rev. Sci. Instrum.* **68**(9), 3277–3295 (1997).
9. L. Xu, E. Zeek, and R. Trebino, "Simulations of frequency-resolved optical gating for measuring very complex pulses," *J. Opt. Soc. Am. B* **25**(6), 70–80 (2008).
10. P. O'Shea, M. Kimmel, X. Gu, and R. Trebino, "Highly simplified device for ultrashort-pulse measurement," *Opt. Lett.* **26**(12), 932–934 (2001).
11. D. Meshulach, D. Yelin, and Y. Silberberg, "Real-time spatial-spectral interference measurements of ultrashort optical pulses," *J. Opt. Soc. Am. B* **14**(8), 2095–2098 (1997).
12. C. Iaconis and I. A. Walmsley, "Spectral phase interferometry for direct electric-field reconstruction of ultrashort optical pulses," *Opt. Lett.* **23**(10), 792–794 (1998).

13. P. Bowlan, P. Gabolde, A. Shreenath, K. McGresham, R. Trebino, and S. Akturk, "Crossed-beam spectral interferometry: a simple, high-spectral-resolution method for completely characterizing complex ultrashort pulses in real time," *Opt. Express* **14**(24), 11892–11900 (2006).
14. K. W. DeLong, D. N. Fittinghoff, and R. Trebino, "Practical issues in ultrashort-laser-pulse measurement using frequency-resolved optical gating," *IEEE J. Quantum Electron.* **32**(7), 1253–1264 (1996).
15. B. H. Kolner, "Space-time duality and the theory of temporal imaging," *IEEE J. Quantum Electron.* **30**(8), 1951–1963 (1994).
16. M. A. Foster, R. Salem, D. F. Geraghty, A. C. Turner-Foster, M. Lipson, and A. L. Gaeta, "Silicon-chip-based ultrafast optical oscilloscope," *Nature* **456**(7218), 81–84 (2008).
17. C. Dorrer, "Single-shot measurement of the electric field of optical waveforms by use of time magnification and heterodyning," *Opt. Lett.* **31**(4), 540–542 (2006).
18. A. Zeytunyan, A. Muradyan, G. Yesayan, L. Mouradian, F. Louradour, and A. Barthélémy, "Generation of broadband similaritons for complete characterization of femtosecond pulses," *Opt. Commun.* **284**(15), 3742–3747 (2011).
19. N. K. Fontaine, R. P. Scott, L. Zhou, F. M. Soares, J. P. Heritage, and S. J. B. Yoo, "Real-time full-field arbitrary optical waveform measurement," *Nat. Photonics* **4**(4), 248–254 (2010).
20. Y. T. Mazurenko, S. E. Putilin, A. G. Spiro, A. G. Beliaev, V. E. Yashin, and S. A. Chizhov, "Ultrafast time-to-space conversion of phase by the method of spectral nonlinear optics," *Opt. Lett.* **21**(21), 1753–1755 (1996).
21. P.-C. Sun, Y. T. Mazurenko, and Y. Fainman, "Femtosecond pulse imaging: ultrafast optical oscilloscope," *J. Opt. Soc. Am. A* **14**(5), 1159–1170 (1997).
22. K. Oba, P. C. Sun, Y. T. Mazurenko, and Y. Fainman, "Femtosecond single-shot correlation system: a time-domain approach," *Appl. Opt.* **38**(17), 3810–3817 (1999).
23. A. M. Kan'an and A. M. Weiner, "Efficient time-to-space conversion of femtosecond optical pulses," *J. Opt. Soc. Am. B* **15**(3), 1242–1245 (1998).
24. D. M. Marom, D. Panasenko, P.-C. Sun, and Y. Fainman, "Linear and nonlinear operation of a time-to-space processor," *J. Opt. Soc. Am. A* **18**(2), 448–458 (2001).
25. J.-H. Chung and A. M. Weiner, "Real-time detection of femtosecond optical pulse sequences via time-to-space conversion in the lightwave communications band," *J. Lightwave Technol.* **21**(12), 3323–3333 (2003).
26. D. M. Marom, D. Panasenko, P.-C. Sun, Y. T. Mazurenko, and Y. Fainman, "Real-time spatial-temporal signal processing with optical nonlinearities," *IEEE J. Sel. Top. Quantum Electron.* **7**(4), 683–693 (2001).
27. D. Shayovitz and D. M. Marom, "High-resolution, background-free, time-to-space conversion by collinearly phase-matched sum-frequency generation," *Opt. Lett.* **36**(11), 1957–1959 (2011).
28. D. Shayovitz, H. Herrmann, W. Sohler, R. Ricken, C. Silberhorn, and D. M. Marom, "High resolution time-to-space conversion of sub-picosecond pulses at 1.55 μm by non-degenerate SFG in PPLN crystal," *Opt. Express* **20**(24), 27388–27395 (2012).
29. D. Shayovitz, H. Herrmann, W. Sohler, R. Ricken, C. Silberhorn, and D. M. Marom, "Time-to-space conversion of ultrafast waveforms at 1.55 μm in a planar periodically poled lithium niobate waveguide," *Opt. Lett.* **38**(22), 4708–4711 (2013).
30. M. T. Kauffman, W. C. Banyai, A. A. Godil, and D. M. Bloom, "Time-to-frequency converter for measuring picosecond optical pulses," *Appl. Phys. Lett.* **64**(3), 270–272 (1994).
31. L. Kh. Mouradian, F. Louradour, V. Messenger, A. Barthélémy, and C. Froehly, "Spectro-temporal imaging of femtosecond events," *IEEE J. Quantum Electron.* **36**(7), 795–801 (2000).
32. G. P. Agrawal, *Fiber-Optic Communication Systems*, 3rd ed. (John Wiley & Sons, 2002).
33. D. Shayovitz, H. Herrmann, W. Sohler, R. Ricken, C. Silberhorn, and D. M. Marom, "Coherent detection of phase modulated ultrashort optical pulses using time-to-space conversion at 1.55 μm ," in *CLEO: 2014*, OSA Technical Digest (online) (Optical Society of America, 2014), paper STu21.3.

1. Introduction

Ultrashort optical pulses are used in many areas of science and technology, for example the investigation of femtosecond time-scale molecular interactions [1, 2], multi-photon microscopy of dynamic biological samples [3], optical data processing [4] and optical communications [5]. Full-field measurement of ultrashort optical pulses is essential for understanding their generation, ascertaining their propagation properties and for pulse shaping applications [6]. For example, temporal phase measurement of a pulse can be used to determine whether it is bandwidth-limited or has undergone dispersive or nonlinear phase distortions. Optoelectronic photodetectors are unable to measure ultrashort (sub-picosecond) pulses, due to their limited electrical bandwidth of ~ 100 GHz in state of the art devices. Pulse measurement techniques are therefore typically based on optical nonlinear phenomena, which are effectively instantaneous on the femtosecond timescale.

The requirements for a successful ultrashort pulse full-field characterization technique include: unambiguous measurement of complex and non-symmetric pulses, single-shot measurement of non-repetitive pulses, a high record length-to-resolution ratio for long and

complex waveforms and algorithm-free phase recovery to minimize post-processing and eliminate the problem of non-convergence.

Among the full-field characterization methods that have been investigated, frequency-resolved optical gating (FROG) [7–10] and spectral interferometry techniques [11–13] such as SPIDER are popular. However, the FROG technique requires a phase recovery algorithm whose run time rapidly increases for larger time-bandwidth product waveforms [14], while SPIDER's record length is limited by spectrometer resolution. Temporal magnification, following the analogy between short pulse dispersive propagation and free-space diffraction [15], can temporally stretch pulses to enable detection by conventional photodetectors [16] or to perform full-field measurement by interferometry in the time [17] or frequency [18] domains. This technique, however, is only single-shot within a time window limited by the stretched reference pulse duration. Optical arbitrary waveform measurement (OAWM) uses spectral slicing and digital coherent detection to achieve a record length-to-resolution ratio of >300,000 [19]. However, the requirement for a stable frequency comb and multiple high-speed receivers and digitizers reduces the practical utility of this method.

2. Full-field measurement by time-to-space conversion

Time-to-space (T-S) conversion realizes full-field measurement of ultrashort optical pulses by transferring the pulse's amplitude and phase information from the temporal domain to a spatial domain image. It is based on sum-frequency generation (SFG) between spatially dispersed signal and reference pulses, resulting in a quasi-monochromatic SFG wave which forms a spatial image of the signal pulse. Preservation of phase in the T-S conversion process has been shown experimentally using displaced image plane observations [20–22], and here we present the first interferometric phase measurements of T-S converted ultrashort pulses. T-S conversion has a number of attractive features including single-shot operation and unambiguous and algorithm-free amplitude and phase measurement.

The principle of operation of T-S conversion [21, 23–26] is illustrated in Fig. 1. The signal and reference pulses, at non-degenerate central wavelengths, are oppositely dispersed by diffraction gratings and are spatially resolved by a Fourier lens, such that their spectra are superimposed at the Fourier plane with equal magnitude and opposite direction linear spatial dispersions. By placing a $\chi^{(2)}$ nonlinear crystal at this plane, SFG occurs between overlapping frequency components of the dispersed signal and reference pulses at each point in space. Due to the matched yet flipped spatial dispersions, a spatially coherent narrow frequency SFG wave is generated all along the crystal aperture, phase-matched across the bandwidth of the dispersed pulses. Temporal walk-off within the nonlinear medium, which can cause distortions in ultrashort pulse measurement, is negligible since the spectrally resolved pulses have extended duration in time.

Time delays between the signal waveform and reference pulse result in linear spectral phases which are converted to linear spatial phases of the quasi-monochromatic SFG wave. A second Fourier lens after the nonlinear crystal converts this linear phase to a transverse spatial shift of the waveform image at the output plane. The instantaneous output field is a quasi-static spatial image of the signal temporal waveform [26]:

$$U_{out}(x, t) = w\left(-\frac{c(t-t_0)}{\alpha}\right) \cdot w\left(\frac{ct}{\alpha}\right) \cdot s\left(\frac{\alpha x}{c} - t_0\right) \otimes r\left(-\frac{\alpha x}{c}\right) \cdot \exp(-j(\omega_s + \omega_r)t) \quad (1)$$

where $s(\bullet)$ and $r(\bullet)$ are the functional forms of the signal and reference input temporal waveforms, mapped to the output plane spatial coordinate x , $w(\bullet)$ is the spatial width of the input beams striking the grating (assumed equal), mapped to the time duration for which the pulse is present and which forms the temporal aperture of the processor and its spectral resolution, $\omega_{S,R}$ are the signal and reference pulse central angular frequencies respectively, α is the dispersion parameter, c is the speed of light, t_0 is the time delay of the signal pulse with respect to the reference pulse and \otimes is the convolution operator. The use of signal and reference pulses at non-degenerate center wavelengths enables spectral filtering of the output

light to block SHG background [27]. The instantaneous time-to-space mapped output field is typically incident on a camera which records the converted time integrated signal intensity without the phase information [23–25, 27–29]. However, the temporal phase of the signal waveform is contained in the output spatial image, which we demonstrate here by recording the interference with a plane wavefront at the same center wavelength. Phase information can then be extracted from the resulting interference fringes.

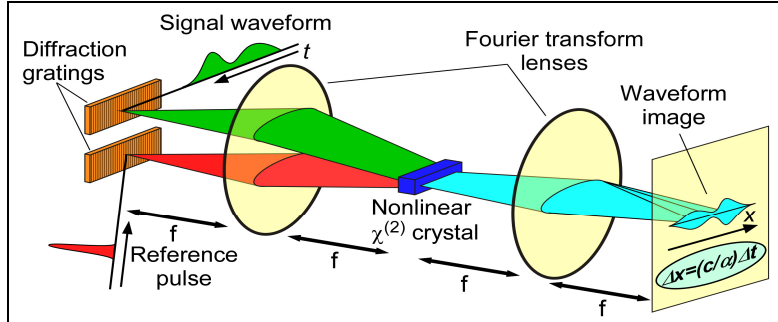


Fig. 1. Time-to-space conversion concept. Time domain information is converted to a spatial image with the temporal coordinate mapped directly to a spatial coordinate: $\Delta x = (c/\alpha)\Delta t$, where c is the speed of light and α is the dispersion parameter (see Eq. (1)). Note that in our experimental setup the signal and reference beams propagated collinearly in the nonlinear crystal, whereas here they are shown at crossed angles for clarity.

It is interesting to note the parallels between time-to-space conversion and time-to-frequency (T-F) conversion [15–18, 30, 31]. T-S conversion mixes the spatially dispersed temporal frequency components of the signal and reference pulses, converting the temporal frequency information to spatial frequencies, and then optically Fourier transforms the spatial frequency information to obtain a space-domain image of the temporal waveform. T-F conversion mixes the temporally dispersed frequency components of chirped signal and reference pulses, imprinting the signal pulse envelope shape onto the generated spectrum. Following this, further chromatic dispersion is applied to temporally resolve the spectral components for photodetection of the temporal intensity profile [16], or instead the T-F spectrum can be immediately measured with a spectrometer [30, 31]. The update rate of this measurement is limited in the first case by the temporal magnification factor and in the second case by the time-integrating spectrometer. T-S conversion, on the other hand, alleviates the temporal resolution problem of short pulse measurement by transferring the time domain envelope to a quasi-static spatial image, which can be recorded with high spatial resolution. The update rate of this measurement is determined by the T-S spectral resolution and by the reference pulse repetition rate, allowing for single-shot recording of long temporal waveforms (see the discussion in section 4).

3. Experiment and results

Figure 2 shows our experimental setup. A mode-locked laser (MLL) generated ~ 100 fs bandwidth-limited pulses at 810 nm with a repetition rate of 80.2 MHz. These were converted by an optical parametric oscillator (OPO) to 'signal' pulses at 1550 nm central wavelength (beam path shown in green) and 'reference' pulses at 1697 nm (shown in red). The signal pulse was directed to one of two phase modulation blocks, resulting in either the generation of a pulse pair with relative phase modulation or a single pulse with quadratic spectral phase modulation. The linear phase modulation block (Fig. 2(b)) consisted of an unbalanced Mach-Zehnder interferometer producing two pulse copies, where one copy passed through a 1 mm thick rotatable glass slide, generating $s(t) = p(t) + p(t-T_0)\exp(j\phi)$, where T_0 is the fixed time delay and ϕ is the modulated phase. The quadratic phase modulation block (Fig. 2(c)) comprised an imaging four-pass pulse stretcher which applied controllable chromatic dispersion, resulting in either positive, negative or zero frequency chirped pulse: $s(t) = \exp(-$

$(1 + jC)t^2/2\tau^2)$, where C is a dimensionless chirp parameter and 2τ is the full-width of the transform limited Gaussian shape pulse measured at e^{-1} intensity points [32]. The modulated signal pulse is then retimed to the reference pulse by a delay line, to coincide at the nonlinear crystal.

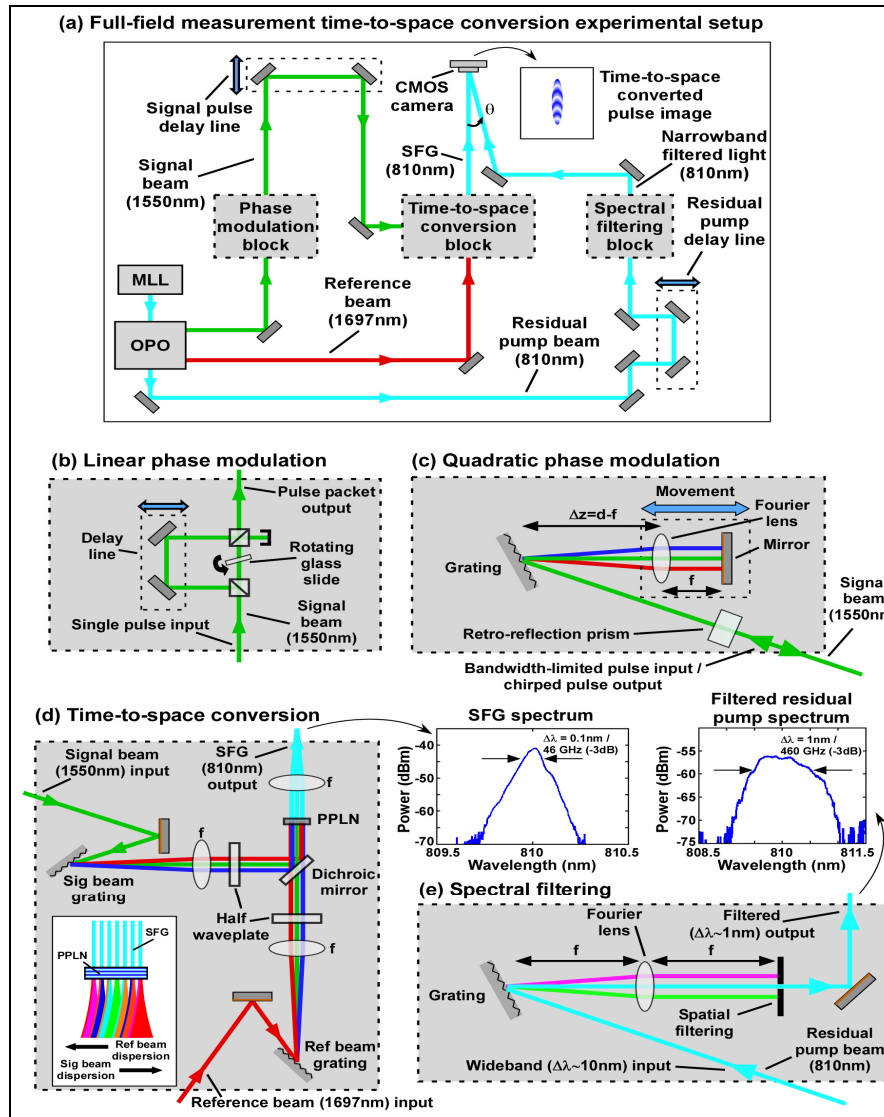


Fig. 2. Full-field measurement time-to-space conversion experimental setup. (a) Overall setup (MLL, mode-locked laser; OPO, optical parametric oscillator; SFG, sum-frequency generation); note that the filtered residual pump beam is incident on the camera at a small angle from above i.e. from out of the plane of the paper. (b) Linear phase modulation block. (c) Quadratic phase modulation block. (d) Time-to-space conversion block (f , Fourier lens; PPLN, periodically-poled lithium niobate). (e) Spectral filtering block for generating the interferogram reference plane wave. The SFG and filtered residual pump spectra are also shown.

The signal pulse was then spatially dispersed by a first diffraction grating (1100 line pairs/mm) and 75 mm focal length Fourier lens (Fig. 2(d)). At the same time the non-modulated reference pulse was given an equal but opposite spatial dispersion by a second diffraction grating (1000 line pairs/mm) and another 75 mm Fourier lens. The two dispersed

pulses were superimposed by a dichroic mirror and were incident on a periodically-poled lithium niobate (PPLN) nonlinear crystal located at the focal plane (see inset in Fig. 2(d)). The PPLN had a poling period of 20.3 μm and dimensions of 12 mm and 8 mm in the spatial dispersion direction and light propagation direction, respectively. The Rayleigh length of the focused signal and reference spectral components inside the PPLN was estimated as ~ 1 mm by measuring the spectral resolution and spatial dispersion of the light at the Fourier plane.

The signal and reference beams' average powers at the PPLN entrance face were measured as 82 mW and 95 mW respectively, resulting in pulse energies of 1 nJ and 1.2 nJ and peak powers of 22 W and 27 W respectively. The peak powers were calculated assuming that the dispersed signal and reference pulses at the Fourier plane were stretched through the time window, which was measured as 46 ps (FWHM). Phase-matched SFG at each point in space resulted in an up-converted output beam centered at 810 nm with a -3dB bandwidth of 0.1 nm (spectrum shown in Fig. 2).

As noted earlier, temporal walkoff due to group velocity mismatch (GVM) between the fundamental and SFG short pulses in a dispersive nonlinear medium can result in distortion of the output signal. For T-S conversion, however, SFG occurs between spatially dispersed pulses, where the spectral bandwidth present at each point in space along the nonlinear crystal aperture is greatly reduced. This effectively transforms the SFG interaction from one between ultrashort pulses subject to large temporal walkoff, into one between multiple quasi-monochromatic beamlets of light, each centered at a different frequency, which experience negligible temporal walkoff. For lithium niobate the GVM between the longest wavelength pulse (the reference pulse at 1697 nm) and the shortest wavelength pulse (the SFG pulse at 810 nm) is 140 fs/mm. Since the SFG interaction length in the PPLN was ~ 1 mm, this results in a temporal walkoff of 0.3% of the 46 ps time window (i.e. the stretched pulse duration).

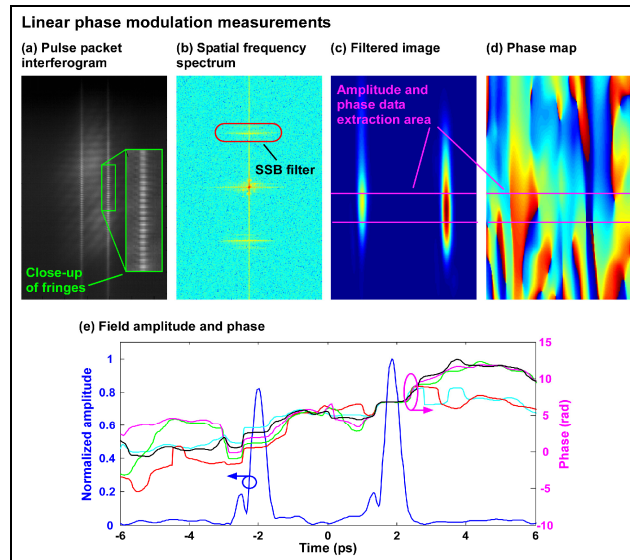


Fig. 3. Pulse packet full-field measurement. (a) Time-to-space converted pulse packet with close-up of the interference fringes. (b) Spatial frequency spectrum of the pulse packet with SSB filter indicated. (c) Inverse Fourier transform of the filtered image. (d) Recovered phase map. (e) Amplitude (blue) and phase (various colors) data taken from the region delimited by pink lines in (c) and (d). Five successive phase measurements are shown, each taken at a linearly increasing applied phase. The normalized field amplitude did not change significantly between successive measurements, so only one amplitude profile is shown here (taken from the same interferogram recording as the light blue line phase profile).

The SFG average beam power emerging from the PPLN was 45 μW (measured for the single unchirped signal pulse case). A 200 mm focal length output Fourier lens focused the SFG light onto a CMOS camera which recorded the pulse image. Next, we interfered the

pulse image with a plane wave having the same center wavelength as the SFG pulse, to extract the phase information. This reference plane wave was generated by spectrally filtering the MLL residual pump pulse exiting the OPO (Fig. 2(e)). The -3dB bandwidth of the filtered residual pump pulse was 1 nm (spectrum shown in Fig. 2). Another delay line temporally overlapped the filtered residual pump pulse and the SFG pulse on arrival at the camera. The reference wave was incident on the camera from above at a small angle to the SFG beam, resulting in the formation of stable interference fringes [33]. Figure 3(a) shows a T-S converted pulse packet interferogram, with fringes clearly visible. By applying single-sideband (SSB) filtering to the image's Fourier transform (Fig. 3(b)) and an inverse Fourier transform (Fig. 3(c)), both the field amplitude and phase were recovered (Figs. 3(d) and 3(e)). Successive phase measurements, shown in different colors in Fig. 3(e), recorded the phase shift of the modulated pulse. Note the flat phase over the two pulse envelopes, with the unmodulated pulse phase staying constant whilst the modulated pulse phase varies with each successive measurement. The small pre-pulses appearing immediately before each of the two main pulse peaks are time-to-space imaging aberrations due to distortions in the temporal intensity envelope of the idler (reference) pulse exiting the OPO.

The quadratic phase modulation experiment is shown in Fig. 4. Figure 4(a) shows an image of a negatively chirped pulse with curved interference fringes. The spatial frequency spectrum, SSB filtered pulse image and recovered phase are shown in Figs. 4(b)-(d), and the time-varying field and phase in Fig. 4(e). In this example a parabolic fit to the phase of the 1.5 ps pulse (FWHM of the intensity envelope) results in a dimensionless chirp parameter of -2 . Measurements were made of positively chirped, bandwidth-limited and negatively chirped pulses. Figure 5 shows pulse duration and chirp parameter values for varying pulse stretcher offsets. Linear variation in pulse chirp with increasing pulse stretcher grating – lens offset can be seen, as well as the evolving pulse duration. The error bars are estimated from confidence bounds on the free parameters of the Gaussian and parabolic fits to the measured amplitude and phase respectively. Note that the chirp measurement error increases for smaller chirp values as the phase becomes flatter and the parabolic fit is less applicable. On the other hand the FWHM duration measurement error decreases for the less strongly stretched pulses, since the offset pulse stretcher introduces some distortions to the pulse envelope.

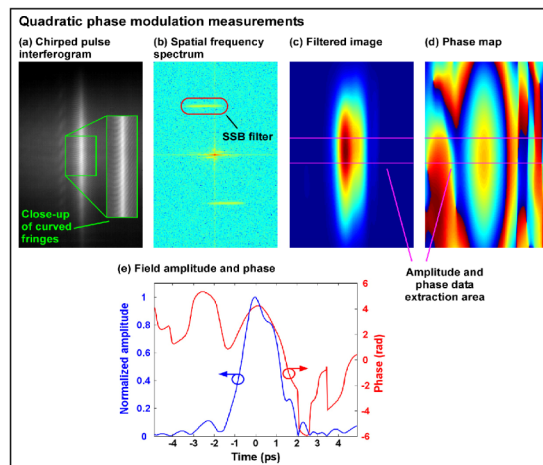


Fig. 4. Chirped pulse full-field measurement. (a) Time-to-space converted negatively chirped pulse interferogram. (b) Spatial frequency spectrum of pulse image. (c) SSB filtered image. (d) Recovered phase map showing quadratic phase variation over the pulse envelope. (e) Pulse field amplitude (blue) and phase (red) with a FWHM pulse duration of $\sim 1.5\text{ ps}$ and chirp parameter of -2 . Note that the distortion of the pulse shape seen in (c) and (e) is believed to be due to spatial distortions and spatio-temporal coupling in the pulse stretcher.

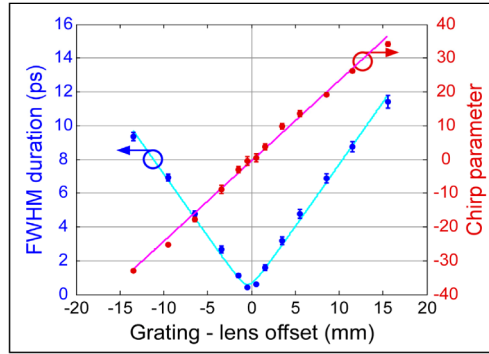


Fig. 5. Measured FWHM pulse duration (blue) and chirp (red) with varying pulse stretcher grating - lens offset, showing Gaussian beam radius evolution and linear fits respectively. The measured chirp clearly shows a linear variation with grating - lens offset. The grating - lens offset zero point (pulse stretcher null position) was determined by the fit to the pulse duration measurements.

4. Discussion and conclusion

The interferogram recording of time-to-space converted ultrashort waveforms reported here operated in real-time and allowed full-field reconstruction without resorting to complex algorithms for phase retrieval. We next discuss the system attributes of our processor.

An important parameter for a waveform measurement technique is the record length-to-resolution ratio, which determines the longest and most complex waveform that can be accurately measured. For T-S conversion the record length is set by the processor's time window, determined by the incident beam sizes on the diffraction gratings. As the time window is extended, by increasing the input beam size, the spectral resolution of the dispersive arrangement is refined and the resultant SFG signal bandwidth is reduced, which allows us to easily record a stable interferogram. We witness the fundamental inverse relationship between time window of operation and spectral bandwidth. In the experiment reported here the SFG bandwidth was measured as 46 GHz (-3dB), roughly in line with our 46 ps time window. In our experiment we acquire the interferogram with a camera operating at several ms integration times, thereby integrating over multiple, repetitive and identical converted signals, which still qualifies as real-time operation. Single-shot operation of the technique can be performed by using a lower repetition pulse source or time-gating a fast one such that a single pulse is incident on the image sensor within its integration time.

The temporal resolution of T-S conversion is determined by the reference pulse duration, as witnessed by the convolution operation in Eq. (1). Temporal features of the signal waveform that are shorter than the reference pulse duration will not be resolved. In our experiment the reference pulse duration was approximately 210 fs (FWHM) and the shortest T-S converted signal pulse was measured as 440 (± 80) fs; this is the temporal resolution achieved in the work reported here. Whilst the reference pulse duration sets a fundamental limit on temporal resolution, an additional criterion is introduced by the pixel density on the image acquisition device. To properly record and maintain system resolution, we require that the pixel pitch be much smaller than the minimal spot size of a converted transform-limited ultrashort optical pulse. We may vary this spot size by selection of output Fourier lenses of different focal lengths.

As can be appreciated from the preceding discussion, some flexibility in determining the main performance parameters of T-S conversion can be afforded by changing aspects of the optical setup, such as the signal and reference beam sizes at the diffraction gratings, the reference pulse duration, and the output Fourier lens focal length. The conversion efficiency is also impacted by these choices, but this is not the main focus of this paper. Finally we note

that T-S conversion is not a self-referencing technique since it requires a previously characterized reference pulse.

In conclusion, we have demonstrated full-field recovery by interferogram optical recording of ultrafast waveforms by time-to-space conversion. The temporal amplitude and phase were measured for bandwidth-limited and positively and negatively chirped pulses varying in duration from 0.5 ps to 10 ps. This technique may complement existing ultrashort pulse measurement methods such as FROG, which relies on an increasingly heavy algorithm for phase recovery of high time-bandwidth product measured waveforms [14]. Time-to-space conversion may be considered particularly for applications requiring algorithm-free and real-time measurement of complex waveforms with high record length-to-resolution ratio.